*Korean J. Chem. Eng.*, 34(1), 234-244 (2017)
DOI: 10.1007/s11814-016-0259-3

pISSN: 0256-1115
eISSN: 1975-7220

# Characterization of bare and modified nano-zirconium oxide ($ZrO_2$) and their applications as adsorbents for the removal of bivalent heavy metals

**Shahriar Mahdavi*,†, Nadereh Amini*, Hajar Merrikhpour**, and Davoud Akhzari*****

*Department of Soil Science, College of Agriculture, Malayer University, Malayer, Iran
**College of Agriculture, University of Sayyed Jamaleddin Asadabadi, Asadabad, Hamedan, Iran
***Department of Watershed and Rangeland Management, Faculty of Natural Resources and Environment, Malayer University, Malayer, Iran
(*Received 23 April 2016 • accepted 9 September 2016*)

**Abstract**–The ability of nano-$ZrO_2$ and modified nano-$ZrO_2$ with humic acid ($ZrO_2$-H) to remove $Cd^{2+}$, $Cu^{2+}$ and $Ni^{2+}$ from aqueous media has been tested by batch sorption studies varying the contact time, initial metal concentration, initial solution pH, sorbent dosage and temperature to understand the adsorption behavior of these metals through adsorption kinetics and isotherms. The bare nanoparticles (NPs) and modified NPs (MNPs) were characterized using X-ray powder diffraction (XRD), SEM-EDX, FTIR to determine the phase, average grain size, morphology, surfacial elemental compounds and functional groups of NPs and MNPs. The pH of the solutions and the temperature controlled the adsorption of metal ions by NPs and MNPs as well as maximum uptake occurred in the first 120 min of reaction in almost all metals. The kinetics of adsorption followed a pseudo-second-order rate equation ($R^2$>0.97) and the isotherms were well described by the Freundlich model in $Cd^{2+}$ and $Cu^{2+}$, but in $Ni^{2+}$ isotherms were better described by Langmuir model. The adsorption of metals onto almost all NPs and MNPs were spontaneous and endothermic in nature. Among the three metals, $Cd^{2+}$ showed more preference towards the sites on $ZrO_2$ and $ZrO_2$-H than $Cu^{2+}$ and $Ni^{2+}$. This study reveals that $ZrO_2$ and $ZrO_2$-H are effective adsorbents in removing $Cd^{2+}$, $Cu^{2+}$ and $Ni^{2+}$ from the aqueous environment with an adsorptive capacity of 46.2, 59.7, 39.5, 29.7, 9.2 and 16.7 $mg \cdot g^{-1}$, respectively.

Keywords: $ZrO_2$ Nanoparticles, Heavy Metals, Water, Sorbent

## INTRODUCTION

Water is one of the world's most abundant resources, but only 2.5% of the world's water is fresh. More than two-thirds of this amount is unavailable for human use, since it exists in glaciers, snow, ice and permafrost [1]. Therefore, the contamination of the limited fresh water resources has become a major global environmental and human health concern as more and more countries become industrialized [2].

The continuous release of various contaminants such as heavy metals and organic compounds into the water causes growing concern to the whole world [1]. Heavy metals are particularly problematic since, unlike most organic contaminants, they are non-degradable and can accumulate in water bodies, posing a great threat to both human health and ecological environment [3]. The most common heavy metals mainly include mercury, cadmium, lead, chromium, arsenic, zinc, copper, nickel, cobalt, and so forth. These metals ions can make toxicities and cause serious side effects toward human health [3,4]. Urbanization, industrial development, and heavy traffic result in the contamination of water with heavy metals [5,6]. Copper ($Cu^{2+}$) is an essential element in many biological systems, which plays an important role in carbohydrate and lipid metabolisms. In general, copper with nearly 40 $\mu g\ L^{-1}$ is required for the normal metabolism of various living organisms; however, at higher levels, it is considered to be toxic and severe intoxication will mainly affect the blood and kidneys [7]. Cadmium ($Cd^{2+}$) is also one of the most hazardous elements to the human health with no essential biological functions and it can have adverse effects on the metabolic processes of human beings. The World Health Organization (WHO) has established 3 $\mu g\ L^{-1}$ as the maximum permissible limits for cadmium in drinking water [8]. Nickel ($Ni^{2+}$), among the first row of transition metals, is a moderately toxic element and the inhalation of this metal and its compounds can lead to serious problems including cancer of respiratory system [9]. The WHO requires that nickel in drinking water should not exceed 0.5 $mgL^{-1}$ [10]. To date, various methods have been used for water remediation, which include ion exchange, biosorption, activated carbon sorption, solvent extraction, mechanical filtration precipitation, coagulation, and adsorption [10,11]. Although these methods have been shown to be effective for the remediation of heavy metals, many of the aforementioned methods are either costly or complex to implement. Adsorption, on the other hand, is relatively inexpensive, attractive and easy to implement [2,5,12,13]. In addition, nanomaterials-based processes are becoming promising options for applications in water treatment [14-17].

The adsorption technique is the most frequently studied method to purify water. Sorption is the loss of ions from the solution phase to the solid phase. Sorption, in fact, describes a group of processes

†To whom correspondence should be addressed.
E-mail: smahdaviha@yahoo.com, sh.mahdavi@malayeru.ac.ir

including adsorption, surface precipitation and absorption (fixation) reactions, which are collectively referred to as "sorption," a general term that should be used when the metal retention mechanism at the oxide surface is unknown [18]. Basically, adsorption is a mass transfer process by which a substance is transferred from the liquid phase to the surface of a solid and becomes bound by physical and/or chemical interactions. Various low-cost adsorbents, derived from agricultural waste, industrial by-products, natural materials, or modified biopolymers, have been recently developed and applied in the removal of heavy metals from metal-contaminated waste water. Technical applicability and cost-effectiveness are the key factors that play major roles in the selection of the most suitable adsorbent to treat waste water [19]. In recent decades, nano-sorbent has been an innovative technology that employs nanoparticles to recover heavy metals from aqueous solutions. It has advantages over other wastewater treatment technologies, since it is a high-efficient and eco-friendly technology [8,14,20-22]. To improve the sorption characteristics of nanoparticles and to enhance their capacity for metal ion uptake, many researchers have chemically modified the NPs by inorganic/organic agents such as thiosalicylhydrazide, 3-Mercaptopropionic acid, Carboxyl, humic acid, acrylic acid (AA) and acrylonitrile (AN) [23-26]. The objective of the present work was to investigate the adsorption potential of the nano zirconium oxide ($ZrO_2$) for the removal of $Cd^{2+}$, $Cu^{2+}$ and $Ni^{2+}$ in individual solutions. In this paper, we modified zirconium oxide with humic acid ($ZrO_2$-H) and studied the adsorption selectivity to $Cd^{2+}$, $Cu^{2+}$ and $Ni^{2+}$ with two NPs: $ZrO_2$ and $ZrO_2$-H. The effect of pH, contact time, temperature and adsorbent dosage on $Cd^{2+}$, $Cu^{2+}$ and $Ni^{2+}$ adsorption capacity of bare and modified zirconium oxide was studied. Furthermore, the kinetics, isotherm models, desorption and spectroscopic analysis such as SEM-EDX, XRD, and FTIR were introduced to study $Cd^{2+}$, $Cu^{2+}$ and $Ni^{2+}$ adsorption mechanism.

## MATERIALS AND METHODS

### 1. Reagents and Chemicals

All chemicals and reagents were analytical grade. Copper chloride ($CuCl_2{\cdot}2H_2O$), cadmium chloride ($CdCl_2{\cdot}2.5H_2O$), and nickel chloride ($NiCl_2$), were purchased from Merck. Humic acid was purchased from Aldrich (Sigma-Aldrich Inc., St. Louis, MO, USA).

### 2. Apparatus

A Varian Spectra AA 220 flame atomic absorption spectrophotometer (FAAS) was used for the determination of the metal ions concentration. A Jenway (UK) model 3020 pH meter with a combined glass electrode was used after calibration against standard Merck buffers for pH determinations. NPs were characterized by X-ray diffraction (XRD, XMD300, Unisantis, CuKa radiation) and scanning electron microscopy was coupled with energy disperse X-ray (SEM-EDX, CamScan MV2300 and Philips XL30) to study their crystallinity, morphology, size, and surficial elemental composition. Fourier transform infrared (FT-IR) spectra were obtained with a Perkin-Elmer, GX, USA FT-IR spectrophotometer using KBr pellet method. The spectra obtained in the range 400-4,000 $cm^{-1}$ were analyzed. A sonicator (Elmasonic, S30H) was used for sonication.

### 3. Functionalization of $ZrO_2$

Humic acid (HA) stock solution (500 mg $L^{-1}$) was prepared according to the method employed by Mahdavi et al., (2015) method [27]. The NPs (0.5 g) were mixed with 30 mL of HA solution at 70 °C and sonicated for 6 hr. Then, the modified-$ZrO_2$ ($ZrO_2$-H) was filtered off and washed with 30 mL of deionized water three times. $ZrO_2$-H was obtained after drying in air.

### 4. Point of Zero Charge (pHpzc) and Zeta Potential

The pH of the point of zero charge, $pH_{PZC}$, that is, the pH above which the total surface of the MNPs are negatively charged, was measured by the so-called pH drift method. For this purpose, 10 mL of the 0.01 mol/L NaCl solutions were adjusted to successive initial values between 2 and 12 by adding either HCl or NaOH, and the four adsorbents ($ZrO_2$ and $ZrO_2$-H) (0.025 g) were added to the solutions. These samples sonicated for 6 h and then were maintained for 42 h. Then, the final pH, after 48 h (25°±1 _C), was measured and plotted against the initial pH. The pH at which the curve crosses the line, pH (final)=pH (initial), was taken as the $pH_{PZC}$ of the two given adsorbents [28]. Zeta potential ($\zeta$ in mV) measurements are measures of the magnitude of charge expressed in the diffuse double layer (DDL) at the plane of slippage. If we set $\zeta \sim \lambda_0$ (given the very short distance of the plane of slippage from the surface) then the relationship between $\zeta$ and the PZC can be simply represented as:

$$\zeta \sim \lambda_0 = 59.2\ (pH_0 - pH) \tag{1}$$

where $\lambda_0$ is surface electrostatic potential, $pH_0$=pH of the PZC, and pH is the pH of the bulk solution [29,30].

### 5. Adsorption and Desorption Studies

The adsorption and desorption studies were conducted in batch mode. Typically, heavy metals adsorption experiments were performed under ambient temperature (25°±1 C) conditions in 50 mL falcon tubes. A weight-to-volume ratio of 1 : 1,000 was adopted for batch experiments. A quantity of 0.025 g (m) of $ZrO_2$ or $ZrO_2$-H was added to 25 mL (v) of a solution containing the heavy metal ions in the appropriate concentration at 1,440 min as contact time. All experiments were performed in triplicate (except for the contact time test that was performed in duplicate) and the mean values were used for the models. For optimization of the adsorption conditions, the quantity of heavy metals ($Cd^{2+}$, $Cu^{2+}$, and $Ni^{2+}$) adsorbed on $ZrO_2$ and $ZrO_2$-H NPs were tested as a function of pH at regular intervals from 2 to 8 and equilibrium liquids were separated from $ZrO_2$ or $ZrO_2$-H by filtration through a 0.45 μm of Sartorius filters (initial concentration of heavy metals was 50 $mg{\cdot}L^{-1}$). The other conditions affecting heavy metals adsorption onto $ZrO_2$ or $ZrO_2$-H were studied by systematically varying the $ZrO_2$ or $ZrO_2$-H dosage (1 to 5 $g{\cdot}L^{-1}$), temperature (15 °C to 40 °C), and contact time (10 min to 1,880 min). To build the adsorption isotherms, the optimum conditions obtained from the mentioned experiment were done to reach equilibrium and $C_0$ has been varied from 10 to 100 $mg{\cdot}L^{-1}$. The amount of $Cd^{2+}$, $Cu^{2+}$, and $Ni^{2+}$ in the solutions before ($c_0$) and after adsorption ($c_e$) was analyzed by a FAAS. The adsorption capacity ($q_e$, mg/g) of heavy metal ions was calculated as:

$$q_e\ (mg{\cdot}L^{-1}) = (C_0 - C_e) \times \frac{V}{m} \tag{2}$$

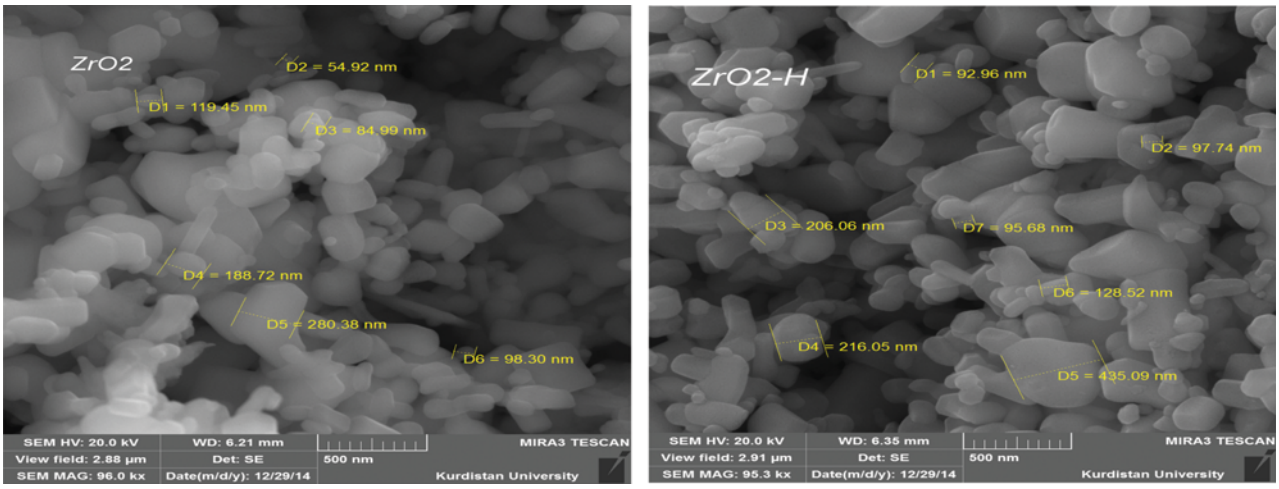


**Fig. 1. SEM images of $ZrO_2$ and $ZrO_2$-H.**

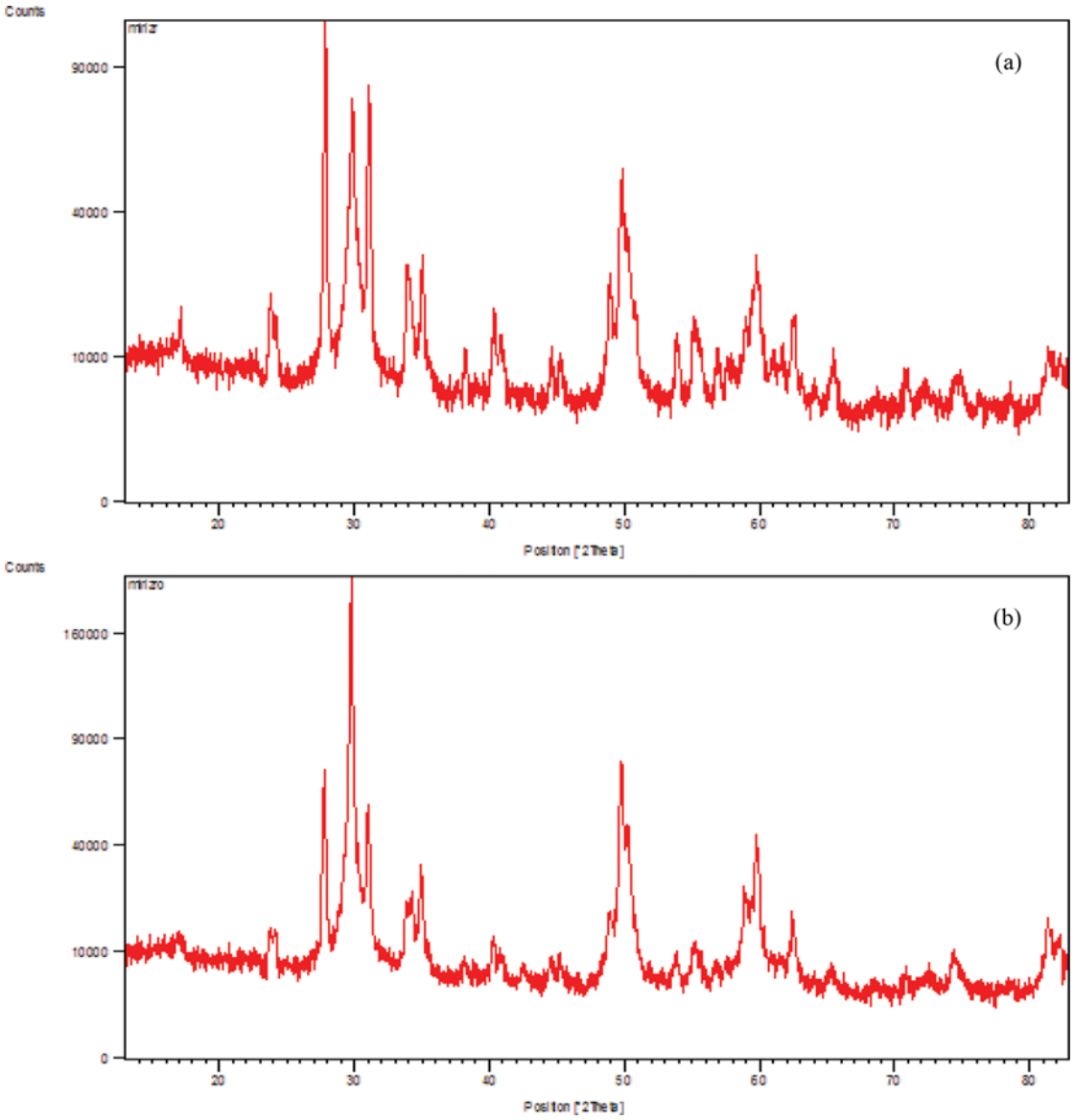


**Fig. 2. In situ XRD patterns of (a) $ZrO_2$ and (b) $ZrO_2$-H.**

To evaluate the feasibility of $ZrO_2$ and $ZrO_2$-H, desorption studies were conducted. Initially, 0.025 g of the initial (10 mg·$L^{-1}$) and final (100 mg·$L^{-1}$) concentration of isotherm points was separated and washed several times with deionized water to remove excess traces of heavy metal ions from isotherm experiments. To elute adsorbed heavy metals ions, $ZrO_2$ and $ZrO_2$-H were treated with 25 mL $CaCl_2$ (0.01 M) for 1,440 min on shaker-incubator under ambient temperature (25°±1 C) conditions. The desorbed heavy metal ions concentrations were analyzed and desorption was calculated as:

$$\text{Desorption (\%)} = \frac{\text{Concentration of heavy metal ions desorbed by eluent}}{\text{Initial concentration of heavy metal ions adsorbed on adsorbent}} \times 100 \quad (3)$$

## RESULTS AND DISCUSSION

### 1. Characterization of the NPs and MNPs

Fig. 1 shows the SEM images of the $ZrO_2$ and $ZrO_2$-H NPs. As it is clear from the SEM images, the mean diameters of the $ZrO_2$NPs and $ZrO_2$-H are137.8 nm and 133.0 nm, respectively (Table 1). NPs and MNPs have heterogeneous shapes and sizes. The crystallization process was studied by XRD patterns twice on two batches of samples for reproducible results. As shown in Fig. 2, the observed diffraction peaks occurred at $2\theta$=24.0°, 28.0°, 30.2°, 35.0°, 50.4°, 58.9°, and 62.8, which can be readily assigned to a tetragonal phase of $ZrO_2$ and $ZrO_2$-H (JCPDS No. 50-1089) [31,32]. Furthermore, no characteristic peaks from other crystalline impurities were detected by XRD, suggesting the high purity of $ZrO_2$ [31,32]. The average crystal size of each of the NPs was calculated using Scherrer's equation and the full width half maximum (FWHM) of independent

**Table 1. Basic properties of bare and modified NPs**

| NPs | Particle size (nm) | Crystal size (nm) | Zeta potential (mv) | PZC |
|---|---|---|---|---|
| $ZrO_2$ | 137.8 | 38.4 | 45.0 | 4.0 |
| $ZrO_2$-H | 133.0 | 51.7 | 61.6 | 5.0 |

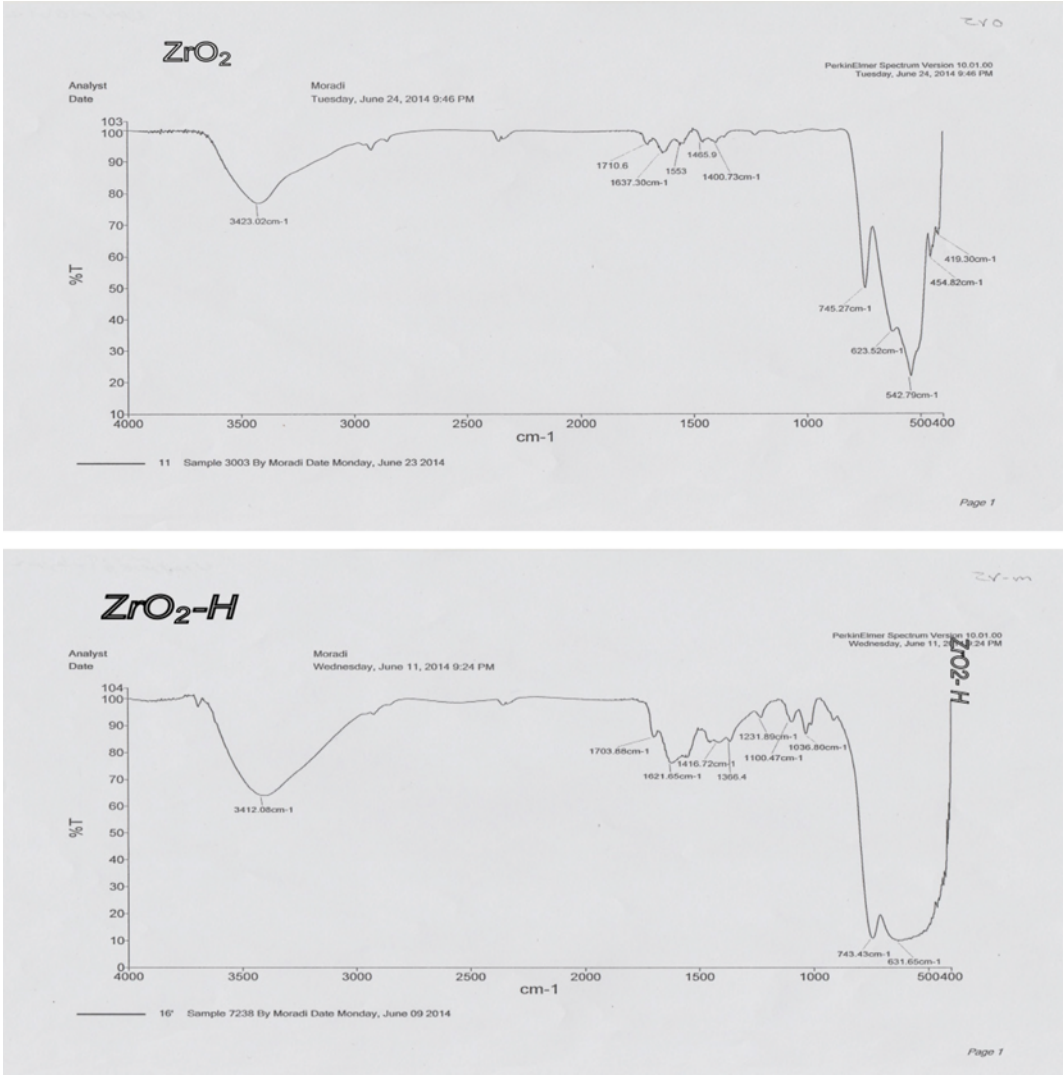


**Fig. 3. Fourier transform infrared (FT-IR) spectra of $ZrO_2$: (a) Bare $ZrO_2$ and (b) $ZrO_2$-H.**

diffraction peaks. Scherrer's equation is provided below:

$$d = \frac{0.9\lambda}{\beta \cos\theta} \quad (4)$$

where d is the NPs diameter, $\lambda$ is the wavelength of the copper X-ray source (1.54 Å), $\beta$ is FWHM of the peak, and $\theta$ is the diffraction angle [33]. Using the Scherrer's method, the average crystal size of $ZrO_2$ and $ZrO_2$-H is represented in Table 1.

FT-IR spectroscopy was used to study the surface functional groups and their interactions with water and metals on the $ZrO_2$ and $ZrO_2$-H surfaces. In Fig. 3, in $ZrO_2$, the vibration band at 3,400-3,430 $cm^{-1}$ is associated with the OH stretching vibrations of water molecules, indicating a higher amount of surface hydroxyl groups, while those at 1,621-1,638 $cm^{-1}$ are associated with their bending mode [34]. A higher amount of surface hydroxyl groups on $ZrO_2$ may show the potential of the compound for the sorption and photocatalytic activity [31,32].

The broad band at 743-542 $cm^{-1}$ in the present case is possibly assigned to Zr-O vibration of $ZrO_2$ [31]. In $ZrO_2$-H, the broader vibration bands at 3,412 $cm^{-1}$ and 1612.6 indicating higher OH groups in comparison with $ZrO_2$ was observed (Fig. 3).

Point zero charges ($pH_{pzc}$) were determined for two adsorbents, i.e., $ZrO_2$ and $ZrO_2$-H. $pH_{pzc}$ is an important property that indicates the electrical neutrality of the adsorbent. From Table 1, it is obvious that the $pH_{pzc}$ shifted from 4.0 ($ZrO_2$) to 5.0 for $ZrO_2$-H. Zeta potential is another parameter that is strongly affected by the media used to stabilize the NPs and prevent their agglomeration. Table 1 shows $ZrO_2$ and $ZrO_2$-H have positive value, indicating that they are positively charged [28], which might decrease the electrostatic attraction between functional groups on $ZrO_2$ and $ZrO_2$-H surfaces and $Cd^{2+}$, $Cu^{2+}$ and $Ni^{2+}$, thus causing the lower adsorption capacity via physical adsorption [35].

**2. Sorption Study**

2-1. Effect of Adsorbent Amount

In order to obtain the optimum adsorbents amount, the effect of different amounts of adsorbents on the adsorption quantities of $Cd^{2+}$, $Cu^{2+}$ and $Ni^{2+}$ was presented in Fig. 4. The adsorption results suggest that the adsorption efficiency of $Cd^{2+}$, $Cu^{2+}$ and $Ni^{2+}$ clearly increases with the increase of adsorbent amount at the beginning.

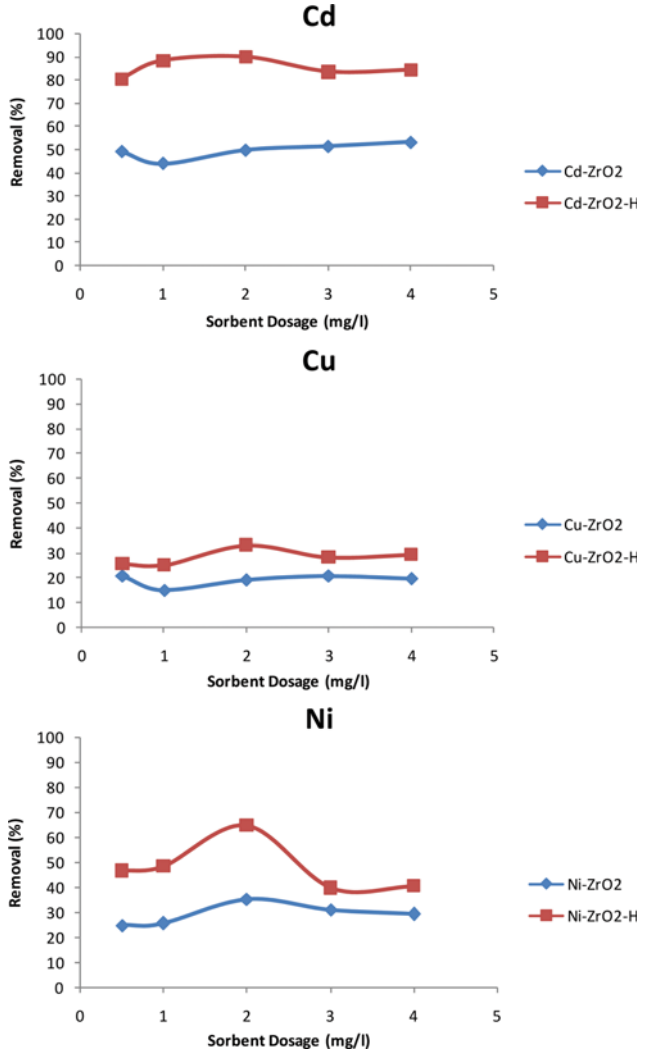


**Fig. 4. Effect of adsorbent dosage on heavy metals adsorption by $ZrO_2$ and $ZrO_2$-H NPs.**

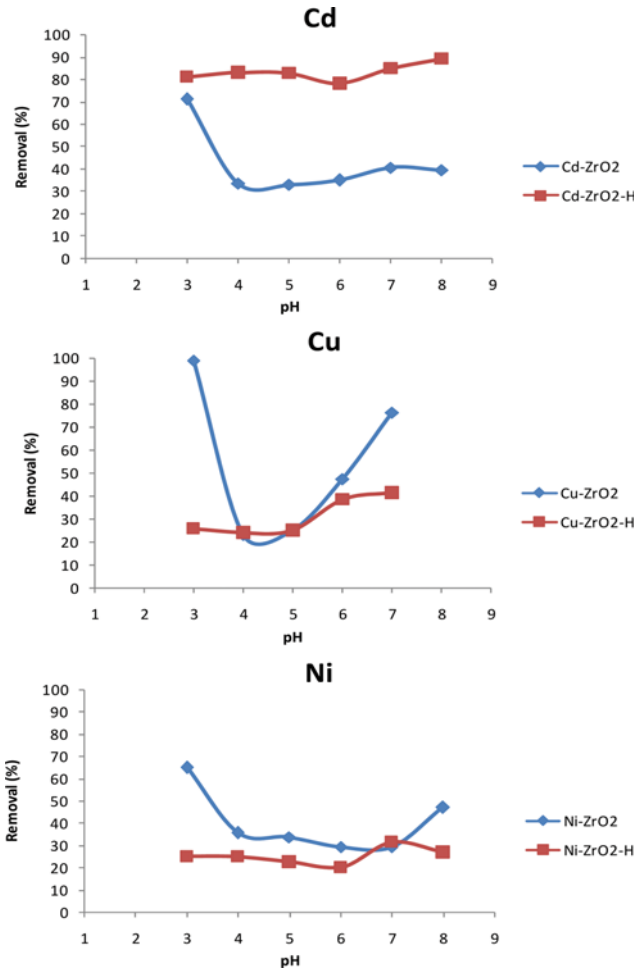


**Fig. 5. Effect of pH value on the adsorption of heavy metals by $ZrO_2$ and $ZrO_2$-H NPs (initial concentrations of heavy metals: 50 $mg \cdot L^{-1}$, sorbent dosage: 1 $g \cdot L^{-1}$, solution volume: 25 ml, time: 24 h, temperature: 25 °C).**

When the amount of the adsorbents was 2 mg·L$^{-1}$ in almost all NPs, the adsorption efficiency reached maximum. However, the adsorption efficiency of $Cd^{2+}$, $Cu^{2+}$ and $Ni^{2+}$ decreases as the amounts of the adsorbents increase from 2 mg·L$^{-1}$ to 5 mg·L$^{-1}$. The reason for this phenomenon was that, the number of unoccupied active adsorption sites grew. Moreover, high dosage may result in the aggregation of the adsorbents [36]. Hence, 2 mg·L$^{-1}$ dosage was chosen in the following experiments.

2-2. Effect of pH

In order to illustrate the effect of the solution pH on the adsorption of $Cd^{2+}$, $Cu^{2+}$ and $Ni^{2+}$ ions, $ZrO_2$ and $ZrO_2$-HNPs were mixed with solutions containing 50 mg·L$^{-1}$ of $Cd^{2+}$, $Cu^{2+}$ and $Ni^{2+}$ at 25 °C and with pH ranging from approximately 3.0±0.1-8.0±0.1. The pH values were adjusted by HCl (0.1 mol·L$^{-1}$) and NaOH (0.1 mol·L$^{-1}$). The equilibrium concentrations of metal ions in the solutions were detected after 24 h. The relationship between the initial pH values and the amount of heavy metals adsorbed on $ZrO_2$ NPs and $ZrO_2$-H adsorbents was shown in Fig. 5. It was observed that the adsorption capacity increased with the increase of solution pH. At lower pH values, the obvious decrease of removals might be attributed to the electrostatic repulsion between the protonated COOH and OH groups of $ZrO_2$-H surface as well as the positive metal ions, but on $ZrO_2$ surface, maximum adsorption occurred at pH=3. As the pH value increased, the adsorption capacity of $Cd^{2+}$, $Cu^{2+}$ and $Ni^{2+}$ ions onto the $ZrO_2$-H was enhanced, since the protonated groups were deprotonated [24,35]. Therefore, $Cd^{2+}$, $Cu^{2+}$ and $Ni^{2+}$ adsorption on the $ZrO_2$-H-nano-adsorbent due to modification process is greater at high pH and increases with the increase of pH.

2-3. Thermodynamic Study and Possible Adsorption Mechanism

The adsorption capacities on $ZrO_2$ NPs and $ZrO_2$-H adsorbents for $Cd^{2+}$, $Cu^{2+}$ and $Ni^{2+}$ were investigated at native pH in the temperature range of 15-40 °C. Thermodynamic studies were conducted, since they can provide information on inherent energetic changes. Parameters such as standard free energy change ($\Delta G^0$), standard enthalpy change ($\Delta H^0$) and standard entropy change ($\Delta S^0$) can be calculated using the following equations [37]:

$$\ln k_c = -\frac{\Delta G^0}{RT} = \frac{\Delta S^0}{R} - \frac{\Delta H^0}{RT} \quad (5)$$

where $K_c$ is the equilibrium constant resulting from the ratio of the

**Table 2. Thermodynamics studies for $Cd^{2+}$ adsorption on $ZrO_2$ and $ZrO_2$-H**

| Cd-$ZrO_2$ | | | |
|---|---|---|---|
| Temperature (°C) | ΔG (KJ·mol$^{-1}$) | ΔH (KJ·mol$^{-1}$) | ΔS$^o$ (J·mol$^{-1}$·K$^{-1}$) |
| 15 | −20.5 | +2.3 | +79.4 |
| 20 | −20.9 | +2.3 | +79.4 |
| 25 | −21.2 | +2.3 | +79.4 |
| 30 | −21.7 | +2.3 | +79.4 |
| 35 | −22.2 | +2.3 | +79.4 |
| 40 | −22.5 | +2.3 | +79.4 |
| Cd-$ZrO_2$-H | | | |
| Temperature (°C) | ΔG (KJ·mol$^{-1}$) | ΔH (KJ·mol$^{-1}$) | ΔS$^o$ (J·mol$^{-1}$·K$^{-1}$) |
| 15 | −26.1 | +19.7 | +160.2 |
| 20 | −27.0 | +19.7 | +160.2 |
| 25 | −28.7 | +19.7 | +160.2 |
| 30 | −29.3 | +19.7 | +160.2 |
| 35 | −29.5 | +19.7 | +160.2 |
| 40 | −30.0 | +19.7 | +160.2 |

**Table 3. Thermodynamics studies for $Cu^{2+}$ adsorption on $ZrO_2$ and $ZrO_2$-H**

| Cu-$ZrO_2$ | | | |
|---|---|---|---|
| Temperature (°C) | ΔG (KJ·mol$^{-1}$) | ΔH (KJ·mol$^{-1}$) | ΔS$^o$ (J·mol$^{-1}$·K$^{-1}$) |
| 15 | −21.7 | +0.6 | +77.8 |
| 20 | −22.3 | +0.6 | +77.8 |
| 25 | −22.3 | +0.6 | +77.8 |
| 30 | −23.2 | +0.6 | +77.8 |
| 35 | −23.2 | +0.6 | +77.8 |
| 40 | −23.7 | +0.6 | +77.8 |
| Cu-$ZrO_2$-H | | | |
| Temperature (°C) | ΔG (KJ·mol$^{-1}$) | ΔH (KJ·mol$^{-1}$) | ΔS$^o$ (J·mol$^{-1}$·K$^{-1}$) |
| 15 | −20.2 | +3.3 | +58.6 |
| 20 | −20.4 | +3.3 | +58.6 |
| 25 | −20.9 | +3.3 | +58.6 |
| 30 | −21.1 | +3.3 | +58.6 |
| 35 | −21.2 | +3.3 | +58.6 |
| 40 | −21.7 | +3.3 | +58.6 |

**Table 4. Thermodynamics studies for $Ni^{2+}$ adsorption on $ZrO_2$ and $ZrO_2$-H**

| Ni-$ZrO_2$ | | | |
|---|---|---|---|
| Temperature (°C) | ΔG (KJ·mol$^{-1}$) | ΔH (KJ·mol$^{-1}$) | ΔS$^o$ (J·mol$^{-1}$·K$^{-1}$) |
| 15 | −20.0 | +6.5 | +95.4 |
| 20 | −21.3 | +6.5 | +95.4 |
| 25 | −21.7 | +6.5 | +95.4 |
| 30 | −22.5 | +6.5 | +95.4 |
| 35 | −22.0 | +6.5 | +95.4 |
| 40 | −23.2 | +6.5 | +95.4 |
| Ni -$ZrO_2$-H | | | |
| Temperature (°C) | ΔG (KJ·mol$^{-1}$) | ΔH (KJ·mol$^{-1}$) | ΔS$^o$ (J·mol$^{-1}$·K$^{-1}$) |
| 15 | −22.8 | −9.4 | +46.7 |
| 20 | −23.3 | −9.4 | +46.7 |
| 25 | −23.3 | −9.4 | +46.7 |
| 30 | −23.3 | −9.4 | +46.7 |
| 35 | −23.7 | −9.4 | +46.7 |
| 40 | −24.2 | −9.4 | +46.7 |

equilibrium sorbed concentrations of $Cd^{2+}$, $Cu^{2+}$ and $Ni^{2+}$ on $ZrO_2$ and $ZrO_2$-H NPs and equilibrium concentration in solution, R is the gas constant (8.314 $J \cdot mol^{-1} \cdot K^{-1}$) and T the absolute temperature. $\Delta G^0$, $\Delta H^0$ and $\Delta S^0$ can be determined experimentally from a plot of $\ln K_c$ versus 1/T and the values of $\Delta G^0$, $\Delta H^0$ and $\Delta S^0$ were collected in Tables 2-4.

The negative values of $\Delta G^0$ indicate the feasibility of the process and spontaneous nature of metal ion adsorption onto $ZrO_2$ and $ZrO_2$-Hnano-adsorbents. In addition, the decrease of $\Delta G^0$ as temperature rises indicated that the adsorption was more favorable at higher temperatures. The positive value of $\Delta H^0$ confirmed the endothermic nature of adsorption, which was also supported by the increase in value of $Cd^{2+}$, $Cu^{2+}$ and $Ni^{2+}$ uptake with the rise in temperature. The positive value of $\Delta S^0$ suggested the increasing randomness at the solid/liquid interface during the adsorption of $Cd^{2+}$, $Cu^{2+}$ and $Ni^{2+}$ ions on $ZrO_2$ and $ZrO_2$-HNPs [15,38] as well as, The positive $\Delta S^0$ value suggests that the adsorption of $Cd^{2+}$, $Cu^{2+}$ and $Ni^{2+}$ occurred spontaneously and a dissociative mechanism was involved in the adsorption processes [37].

2-4. Kinetics of Metals Sorption with the $ZrO_2$ and $ZrO_2$-HNPs

A relationship between an amount of heavy metals bounded with $ZrO_2$ and $ZrO_2$-H NPs and the heavy metals concentration remaining in an aqueous solution is studied by an appropriate sorption kinetics. The analysis of the kinetic data is important to develop an equation, which accurately represents the results and could be used for design purposes. Several kinetic models have been prepared to describe the experimental $Cd^{2+}$, $Cu^{2+}$ and $Ni^{2+}$ sorption data. In this paper, we have compared Lagergren's pseudo-first-order and pseudo-second-order kinetic models. The mathematical representation of the pseudo first order model is as follows [14,15]:

$$\ln(q_e - q_t) = \ln q_e - K_1 t \quad (6)$$

where $q_e$ and $q_t$ are the amount ($mg \cdot g^{-1}$) of heavy metals sorbet at equilibrium and at time t, respectively, and $k_1$ ($min^{-1}$) is the pseudo-first order rate constant. The pseudo-second order model can be is described by the following equation [27,39]:

$$\frac{1}{q_t} = \frac{1}{K_2 q_e^2} + \frac{t}{q_e} \quad (7)$$

The constant $k_2$ ($g \cdot (mg \cdot min)^{-1}$) and the amount of heavy metals adsorbed at equilibrium $q_e$ ($mg \cdot g^{-1}$) can be obtained by plotting $1/q_t$ vs. t.

The obtained results show that the pseudo-second order model illustrate the heavy metals sorption kinetic better than pseudo-first order. Fig. 6 presents the linear time course relationships for heavy metals sorption with $ZrO_2$ NPs and $ZrO_2$-H in the pseudo-second order model. The corresponding parameters of the pseudo-second-order model were listed in Table 5. The adsorption system obeyed the pseudo-second-order kinetic model for the entire adsorption period and thus supported the assumption that the adsorption is probably the chemisorption process [23].

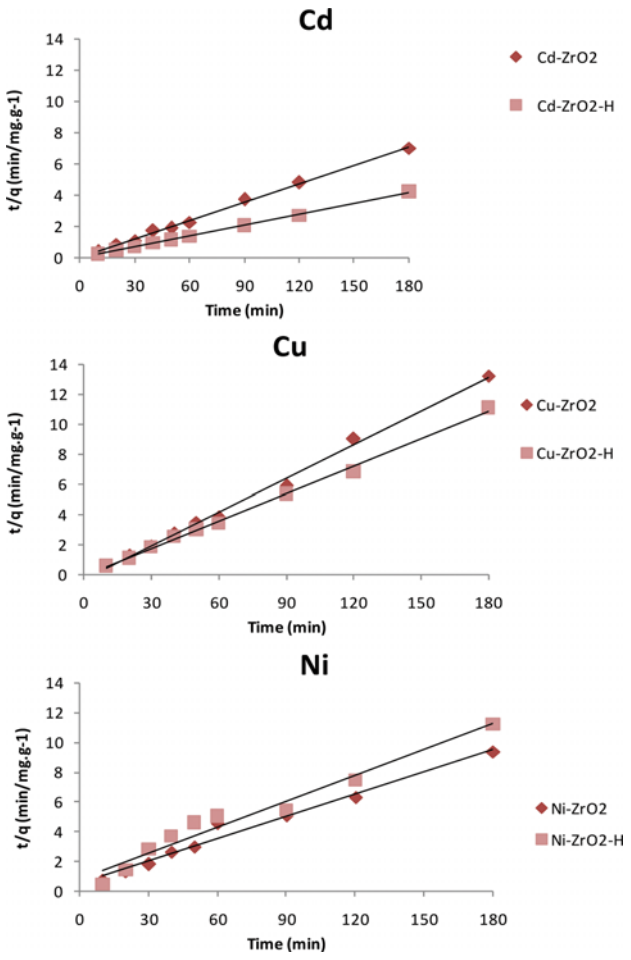


**Fig. 6. Effect of contact time on the extraction of heavy metals by $ZrO_2$ and $ZrO_2$-H NPs, with pseudo second-order adsorption kinetics (conditions: T: 25 °C, initial concentration of heavy metals concentration: 50 $mg \cdot L^{-1}$, sorbent dosage: 1 $g \cdot L^{-1}$).**

**3. Sorption Isotherms**

To understand the adsorption mechanism of $Cd^{2+}$, $Cu^{2+}$ and $Ni^{2+}$ ions on the nano-adsorbent, which is highly important for the design of adsorption systems, the adsorption data were constructed by adsorption isothermal model (Fig. 7). Therefore, both Langmuir and Freundlich adsorption isotherms were employed to normalize the adsorption data. The linear form of the Langmuir equation is shown below [12,33]:

**Table 5. Kinetic parameter of pseudo-second-order model for heavy metals adsorption**

| | $ZrO_2$-H | | | $ZrO_2$ | | |
|---|---|---|---|---|---|---|
| | $R^2$ | $K_2$ ($g \cdot mg^{-1} \cdot min^{-1}$) | $q_e$ ($mg \cdot g^{-1}$) | $R^2$ | $K_2$ ($g \cdot mg^{-1} \cdot min^{-1}$) | $q_e$ ($mg \cdot g^{-1}$) |
| $Cd^{2+}$ | 0.99 | 0.02 | 43.10 | 0.99 | 0.11 | 25.44 |
| $Cu^{2+}$ | 0.99 | 0.05 | 16.55 | 0.99 | 0.01 | 13.44 |
| $Ni^{2+}$ | 0.97 | 0.01 | 16.63 | 0.99 | 0.01 | 19.92 |

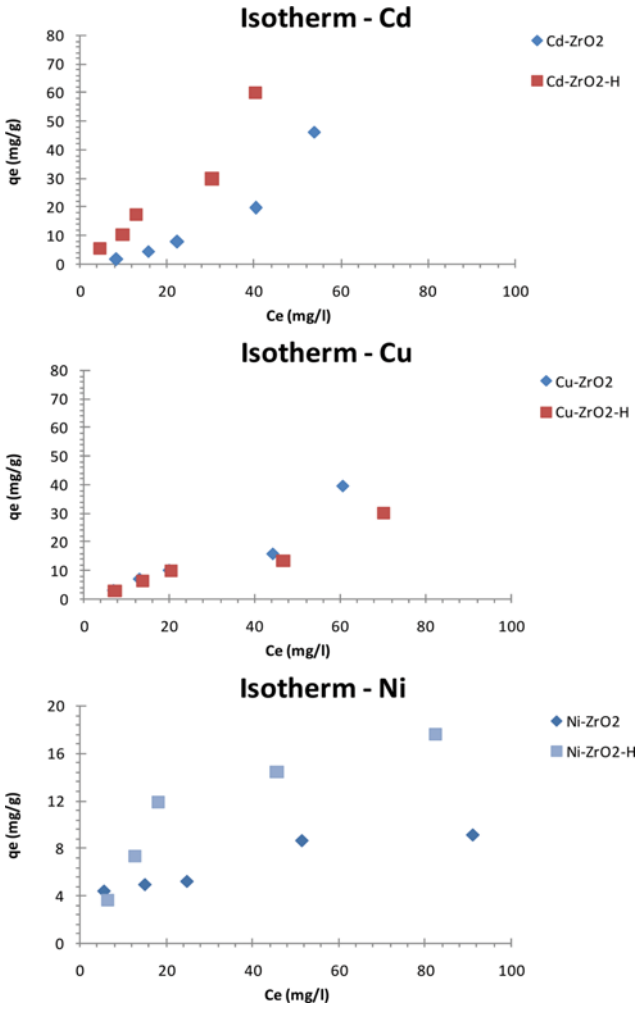


**Fig. 7. Adsorption isotherm of (a) $Cd^{2+}$, $Cu^{2+}$ and (b) $Ni^{2+}$ by $ZrO_2$ and $ZrO_2$-H NPs (contact time: 120 min, adsorbent amount: 2 g·$L^{-1}$, pH: 3, 7 for bare and modified NPs, respectively).**

$$\frac{C_e}{q_e} = \frac{C_e}{q_m} + \frac{1}{q_m K_L} \quad (8)$$

where $q_e$ is the equilibrium concentration of the metals, $q_m$ is the monolayer sorption capacity of the NPs ($ZrO_2$ or $ZrO_2$-H), $K_L$ is a constant related to the binding strength of adsorption, and $C_e$ is the equilibrium metal concentration. By plotting $c_e/q_e$ versus $C_e$ and employing the linearized Langmuir equation, the inverse slope of the line can be used to calculate the capacity of the adsorbent. The estimated $q_m$ and $K_L$ values are presented in Table 6. The correlation coefficient ($R^2$) values for $Ni^{2+}$ on $ZrO_2$ or $ZrO_2$-HNPs indicate that the sorption is well described by the Langmuir model. The Langmuir model predicts that the adsorption of molecule is a monolayer adsorption, with no side interaction among adsorbed molecule. It also assumes that the adsorption of adsorbent surface is uniform [40,41].

The Freundlich model considers the existence of a multi-layered structure. This model is given by the following equation [42]:

$$\text{Log } q_e = \text{Log } k_F + 1/n \text{ Log } C_e \quad (9)$$

Where, $k_F$ ($mg \cdot g^{-1}$) and n are empirical constants (Freundlich constants), $k_F$ is related to the relative adsorption capacities of the adsorbent and n is adsorption intensity. The plots of $\log q_e$ vs $\log C_e$ was straight line and the intercept was related to $k_F$. Adsorption intensity was computed by slope (1/n).

The results showed that the values of $R^2$ for the Freundlich model fitted better than the Langmuir model with $Cd^{2+}$ and $Cu^{2+}$, demonstrating that the adsorption onto $ZrO_2$ or $ZrO_2$-H can be considered to be a multilayer adsorption process. The Freundlich isotherm parameters were calculated, which are summarized in Table 7.

The $ZrO_2$ or $ZrO_2$-H adsorbents were tested for the removal of $Cd^{2+}$, $Cu^{2+}$, and $Ni^{2+}$ from aqueous solutions. Preliminary adsorption studies as presented in Tables 6-7, showed maximum adsorption of $Cd^{2+}$ ions followed by $Cu^{2+}$>$Ni^{2+}$. Here, it is noteworthy that hydrated ionic radii and electronegativity of heavy metal ions play a significant role in controlling adsorption process. The higher hydrated ionic radius induces a quick saturation of adsorption sites, due to a steric hindrance while, greater the electronegativity, greater the affinity of heavy metal ions to bind with the adsorbent surface. The hydrated radii of the studied heavy metal ions are $Ni^{2+}$ (4.04 Å)<$Cu^{2+}$ (4.19 Å)<$Cd^{2+}$ (4.26 Å), while the electronegativity decreases as follows: $Ni^{2+}$ (1.91)>$Cu^{2+}$ (1.90)>$Cd^{2+}$ (1.69). A decrease in hydrated radii and increase in metals electronegativity lead to a

**Table 6. Langmuir and Freundlich isotherm constants**

| Langmuir isotherm | | $R^2$ | $K_L$ ($L \cdot mg^{-1}$) | $q_{max}$ ($mg \cdot g^{-1}$) | Maximum sorption[a] |
|---|---|---|---|---|---|
| $Ni^{2+}$ | $ZrO_2$ | 0.96 | 15.4 | 10.7 | 9.2 |
| | $ZrO_2$-H | 0.96 | 27.8 | 23.7 | 17.6 |

[a]From simple isotherm ($mg \cdot g^{-1}$)

**Table 7. Freundlich isotherm constants**

| Freundlich isotherm | | $R^2$ | n | $K_f$ ($mg \cdot g^{-1}$) | Maximum sorption[a] |
|---|---|---|---|---|---|
| $Cd^{2+}$ | $ZrO_2$ | 0.98 | 0.57 | 26.8 | 46.2 |
| | $ZrO_2$-H | 0.96 | 0.94 | 1.1 | 59.7 |
| $Cu^{2+}$ | $ZrO_2$ | 0.94 | 0.97 | 2.2 | 39.5 |
| | $ZrO_2$-H | 0.95 | 1.05 | 2.2 | 29.7 |

[a]From simple isotherm ($mg \cdot g^{-1}$)

**Table 8. Summary of the investigated $Cd^{2+}$ adsorption capacities of various adsorbents**

| Adsorbent | Capacity/mg $g^{-1}$-$Cd^{2+}$ | Reference |
|---|---|---|
| Thio salicylhydrazide on the surface of $Fe_3O_4$ | 107.5 | [24] |
| Humic acid modified MWCNTs | 18.4 | [44] |
| Nano $TiO_2$ modified with humic acid | 9.9 | [14] |
| Eucalyptus bark | 15 | [45] |
| Carboxyl functionalized magnetite nanoparticles | 45.7 | [21] |
| Iron oxide modified with sewage sludge | 14.7 | [46] |
| Mixture of fly ash and $TiO_2$ | 9.5 | [47] |
| Ethylenediamine functionalized MWCNTs | 25.7 | [34] |
| Flower-like $TiO_2$-graphene oxide | 14.9 | [48] |
| $ZrO_2$ | 46.2 | This study |
| $ZrO_2$-H | 59.7 | This study |

**Table 9. Summary of the investigated $Cu^{2+}$ adsorption capacities of various adsorbents**

| Adsorbent | Capacity/mg $g^{-1}$-$Cu^{2+}$ | Reference |
|---|---|---|
| Amino-functionalized $Fe_3O_4$ nano-adsorbent | 12.4 | [49] |
| Mixture of fly ash and $TiO_2$ | 9.5 | [47] |
| Tree fern | 11.7 | [50] |
| Graphene oxide-chitosan | 25.4 | [51] |
| Carboxyl functionalized magnetite nanoparticles | 44.8 | [21] |
| PVA/$TiO_2$/APTES nanohybrid | 13.1 | [52] |
| Lignin | 22.9 | [53] |
| Hydroxyapatite modified with Humic acid | 41.8 | [54] |
| Thiosalicylhydrazide on the surface of $Fe_3O_4$ | 76.9 | [24] |
| $ZrO_2$ | 29.7 | This study |
| $ZrO_2$-H | 60.9 | This study |

**Table 10. Summary of the investigated $Ni^{2+}$ adsorption capacities of various adsorbents**

| Adsorbent | Capacity/mg $g^{-1}$-$Ni^{2+}$ | Reference |
|---|---|---|
| Alginate beads | 10.9 | [9] |
| Mg-mesoporous alumina | 16.6 | [38] |
| Carbon in alginate bed | 11.5 | [10] |
| Nanoporous silica | 98.0 | [11] |
| MPA@$Fe_3O_4$ MNPs | 42.0 | [23] |
| Coir pith | 9.5 | [55] |
| Hydrous $TiO_2$ | 8.3 | [39] |
| Iron oxide modified with sewage sludge | 7.8 | [46] |
| $ZrO_2$-kaolinite | 8.8 | [56] |
| Activated sludge | 8.8 | [57] |
| $ZrO_2$ | 9.2 | This study |
| $ZrO_2$-H | 17.6 | This study |

growing tendency of the ion for specific adsorption [43]. The comparison of the maximum adsorption capacity with some recent different adsorbents toward $Cd^{2+}$, $Cu^{2+}$, and $Ni^{2+}$ ions are shown in Tables 8-10. The maximum sorption capacity of the present NPs are comparable with the listed other forms of materials. The data clearly clarified that the $ZrO_2$ or $ZrO_2$-HNPs can be used as a highly efficient adsorbent to take up $Cd^{2+}$, $Cu^{2+}$, and $Ni^{2+}$ ions with high adsorption capacity. The low adsorption of $Ni^{2+}$ can be attributed to "hard soft acid base" theory, nickel is an "intermediate" metal that forms less stable complexes, mainly by weaker ionic bonding [10]. Furthermore, the morphology of $ZrO_2$ or $ZrO_2$-H NPs has been changed due to the direct binding of $Cd^{2+}$, $Cu^{2+}$, and $Ni^{2+}$ ions on the surface of $ZrO_2$ and $ZrO_2$-H NPs and this reaction produced different chemical and surface structures. The results of SEM-EDX analysis demonstrated that $Cd^{2+}$, $Cu^{2+}$, and $Ni^{2+}$ ions were indeed in-situ obtained on nano-$ZrO_2$ NPs surfaces (Fig. 8). EDX (Energy

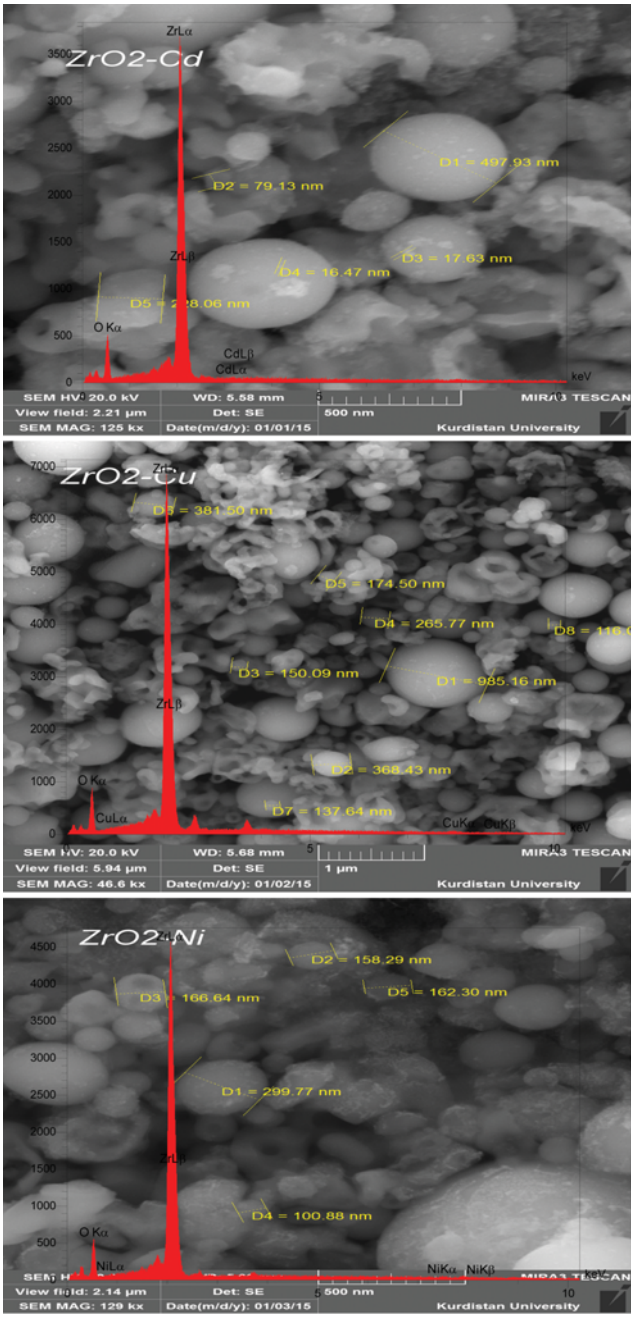


**Fig. 8. SEM-EDX spectra for $ZrO_2$ NPs after adsorption of $Cd^{2+}$, $Cu^{2+}$ and $Ni^{2+}$ and elements detected on $ZrO_2$.**

dispersive X-ray) analysis data confirmed the sorption of $Cd^{2+}$, $Cu^{2+}$, and $Ni^{2+}$ ions on $ZrO_2$ NPs (Fig. 8).

**4. Desorption Experiments**

The stability of adsorbents is an extremely important factor in evaluating their potential applications. Therefore, it is necessary to evaluate adsorbents under proper conditions. In order to investigate the stability capacity of adsorbents, desorption experiments were first performed under batch experimental conditions in the initial and final points of isotherm experiments (10 and 100 $mg{\cdot}L^{-1}$). In this study, $CaCl_2$ (0.01 M) was chosen as the desorbing agent. The most desorption efficiency occurred in 10 $mg{\cdot}L^{-1}$ of the initial

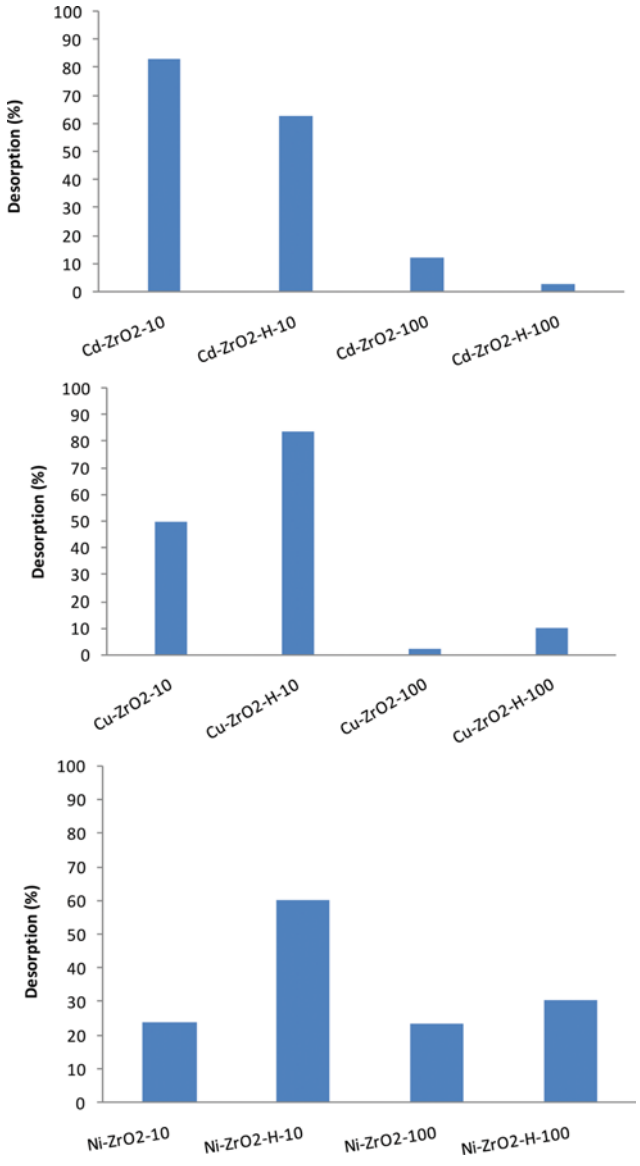


**Fig. 9. Performance of heavy metals desorption using 0.01 M $CaCl_2$.**

concentration of $Cd^{2+}$ in almost all NPs. This phenomenon may be attributed to the reversible process of cationic exchange and mass action phenomena between the $Cd^{2+}$ and nano-adsorbents surfaces and $Ca^{2+}$. The desorption potential of adsorbents was shown in Fig. 9.

## CONCLUSION

In this work, novel nano-adsorbents have been utilized bare and modified with humic acid of $ZrO_2$ NPs for the removal of $Cd^{2+}$, $Cu^{2+}$ and $Ni^{2+}$ ions from aqueous samples. The maximum adsorption capacities of $Cd^{2+}$, $Cu^{2+}$ and $Ni^{2+}$ were found to be 46.2, 29.7, and 9.2 $mg{\cdot}g^{-1}$, in $ZrO_2$ NPs, respectively. In addition, the presence of modified $ZrO_2$ with extending functional groups such as COOH, and OH can significantly improve the adsorption capacity of the adsorbents. These improvements may be due to higher affinity of the COOH, and OH sites of the modified MNPs for complex for-

mation with heavy metal ions via soft-soft interactions. The appropriate characteristics of the modified $ZrO_2$-H such as high adsorption capacity, reusability, easy synthesis, easy separation, and eco-friendly composition make them suitable alternatives to the well-known and widely used adsorbents for the removal of the mentioned heavy metal ions from aqueous samples.

## REFERENCES


1. R. Clarke and J. King, The atlas of water (2004).
2. C. Tamez, R. Hernandez and J. G. Parsons, *Microchem. J.*, **125**, 97 (2015).
3. A. Naeem, M. Saddique, S. Mustafa, S. Tasleem, K. Shah and M. Waseem, *J. Hazard. Mater.*, **172**(1), 124 (2009).
4. W.-W. Tang, G.-M. Zeng, J.-L. Gong, J. Liang, P. Xu, C. Zhang and B. B. Huang, *Sci. Total Environ.*, **468**, 1014 (2014).
5. O. Amiri, H. Emadi, S. S. M. Hosseinpour-Mashkani, M. Sabet and M. M. Rad, *RSC Adv.*, **4**(21), 10990 (2014).
6. H. Merrikhpour and S. Mahdavi, *Heavy metal contamination and solid phase speciation in street dusts*, Archives of Environmental & Occupational Health, 1-10, DOI:10.1080/19338244.2016.1219300.
7. A. B. Tabrizi, *J. Hazard. Mater.*, **139**(2), 260 (2007).
8. M. Behbahani, A. Esrafili, S. Bagheri, S. Radfar, M. K. Bojdi and A. Bagheri, *Measurement*, **51**, 174 (2014).
9. J. Abolhasani, M. Behbahani, *Environ. Monitoring Assessment.*, **187**(1), 1 (2015).
10. W. Jung, B.-H. Jeon, D.-W. Cho, H.-S. Roh, Y. Cho, S.-J. Kim and D. S. Lee, *J. Ind. Eng. Chem.*, **26**, 364 (2015).
11. Z. Hajahmadi, H. Younesi, N. Bahramifar, H. Khakpour and K. Pirzadeh, *Water Res. Ind.*, **11**, 71 (2015).
12. I. Anastopoulos, M. Panagiotou, C. Ehaliotis, P. A. Tarantilis and I. Massas, *Chem. Ecol.*, **31**(8), 724 (2015).
13. Q. Peng, J. Guo, Q. Zhang, J. Xiang, B. Liu, A. Zhou, R. Liu and Y. Tian, *J. Am. Chem. Soc.*, **136**(11), 4113 (2014).
14. S. Mahdavi, *Clean Technologies Environ. Policy*, **18**(1), 81 (2016).
15. S. Mahdavi and D. Akhzari, *Clean Technologies Environ. Policy*, **18**(3), 817 (2016).
16. J.-G. Yu, X.-H. Zhao, L.-Y. Yu, F.-P. Jiao, J.-H. Jiang and X.-Q. Chen, *J. Radioanalytical Nuclear Chem.*, **299**(3), 1155 (2014).
17. Q. Zhang, Q. Du, M. Hua, T. Jiao, F. Gao and B. Pan, *Environ. Sci. Technol.*, **47**(12), 6536 (2013).
18. D. L. Sparks, Environmental Soil Chemistry, Academic Press (2003).
19. M. M. Khin, A. S. Nair, V. J. Babu, R. Murugan and S. Ramakrishna, *Energy Environ. Sci.*, **5**(8), 8075 (2012).
20. A. S. Adeleye, J. R. Conway, K. Garner, Y. Huang, Y. Su and A. A. Keller, *Chem. Eng. J.*, **286**, 640 (2016).
21. B. Al-Rashdi, C. Somerfield and N. Hilal, *Sep. Purif. Rev.*, **40**(3), 209 (2011).
22. S. Mahdavi, A. Afkhami and M. Jalali, *Environ. Earth Sci.*, **73**(8), 4347 (2015).
23. S. Venkateswarlu, S. H. Kumar and N. Jyothi, *Water Res. Ind.*, **12**, 1 (2015).
24. K. Zargoosh, H. Abedini, A. Abdolmaleki and M. R. Molavian, *Ind. Eng. Chem. Res.*, **52**(42), 14944 (2013).
25. J. Shi, H. Li, H. Lu and X. Zhao, *J., Chem. Eng. Data*, **60**(7), 2035 (2015).
26. X. Jin, C. Yu, Y. Li, Y. Qi, L. Yang, G. Zhao and H. Hu, *J. Hazard. Mater.*, **186**(2-3), 1672 (2011).
27. S. Mahdavi, A. Afkhami and H. Merrikhpour, *Clean Technologies Environ. Policy*, **17**(6), 1645 (2015).
28. M. B. McBride, *Environmental chemistry of soils*, Oxford University Press (1994).
29. S. Mahdavi, M. Jalali and A. Afkhami, *Clean Technologies Environ. Policy*, **17**(1), 85 (2015).
30. M. Chappell, *Solid-phase characteristics of engineered nanoparticles*, Nanomaterials: Risks and Benefits: Springer, 111 (2009).
31. N. C. S. Selvam, A. Manikandan, L. J. Kennedy and J. J. Vijaya, *J. Colloid Interface Sci.*, **389**(1), 91 (2013).
32. Y. Zhang, X. Jin, Y. Rong, T. Hsu, D. Jiang and J. Shi, *Mater. Sci. Eng.: A.*, **438**, 399 (2006).
33. C. Tamez, R. Hernandez and J. G. Parsons, *Microchem. J.*, **125**, 97 (2016).
34. Q. Zhang, J. Teng, G. Zou, Q. Peng, Q. Du, T. Jiao and J. Xiang, *Nanoscale.*, **8**(13), 7085 (2016).
35. W. Zhang, L. Meng, G. Mu, M. Zhao, P. Zou and Y. Zhang, *Appl. Surface Sci.*, **378**, 196 (2016).
36. R. B. Nessim, A. R. Bassiouny, H. R. Zaki, M. N. Moawad and K. M. Kandeel, *Chem. Ecol.*, **27**(6), 579 (2011).
37. T. Wang, X. Jin, Z. Chen, M. Megharaj and R. Naidu, *J. Ind. Eng. Chem.*, **20**(5), 3543 (2014).
38. S. Nasirimoghaddam, S. Zeinali and S. Sabbaghi, *J. Ind. Eng. Chem.*, **27**, 79 (2015).
39. T. Jiao, H. Guo, Q. Zhang, Q. Peng, Y. Tang, X. Yan and B. Li, *Scientific Reports*, **5**, 11873 (2015), DOI:10.1038/srep11873.
40. M. E. Essington, Soil and water chemistry: An integrative approach, CRC Press (2015).
41. V. Evangelou, *J. Mole. Liq.*, **211**, 457 (2015).
43. M. Arshadi, M. J. Amiri and S. Mousavi, *Water Res. Ind.*, **6**, 1 (2014).
44. X. Tian, T. Li, K. Yang, Y. Xu, H. Lu and D. Lin, *Chemosphere*, **89**(11), 1316 (2012).
45. I. Ghodbane, L. Nouri, O. Hamdaoui and M. Chiha, *J. Hazard. Mater.*, **152**(1), 148 (2008).
46. T. Phuengprasop, J. Sittiwong and F. Unob, *J. Hazard. Mater.*, **186**(1), 502 (2011).
47. M. Visa and A. Duta, *Chem. Eng. J.*, **223**, 860 (2013).
48. Y.-C. Lee and J.-W. Yang, *J. Ind. Eng. Chem.*, **18**(3), 1178 (2012).
49. S.-H. Huang and D.-H. Chen, *J. Hazard. Mater.*, **163**(1), 174 (2009).
50. Y.-S. Ho, *Water Res.*, **37**(10), 2323 (2003).
51. B. Yu, J. Xu, J.-H. Liu, S.-T. Yang, J. Luo, Q. Zhou, J. Wan, R. Liao, H. Wang and Y. Liu, *J. Environ. Chem. Eng.*, **1**(4), 1044 (2013).
52. S. Abbasizadeh, A. R. Keshtkar and M. A. Mousavian, *J. Ind. Eng. Chem.*, **20**(4), 1656 (2014).
53. X. Guo, S. Zhang and X.-q. Shan, *J. Hazard. Mater.*, **151**(1), 134 (2008).
54. L. Yang, Z. Wei, W. Zhong, J. Cui and W. Wei, *Colloids Surfaces A: Physicochem. Eng. Aspects.*, **490**, 9 (2016).
55. A. Ewecharoen, P. Thiravetyan and W. Nakbanpote, *Chem. Eng. J.*, **137**(2), 181 (2008).
56. K. G. Bhattacharyya and S. S. Gupta, *Colloids Surfaces A: Physicochem. Eng. Aspects.*, **317**(1), 71 (2008).
57. A. Hammaini, F. González, A. Ballester, M. Blázquez and J. Munoz, *J. Environ. Manage.*, **84**(4), 419 (2007).